Technical note: Evaporating water is different from bulk soil water in δ^2H and δ^{18}O

Hongxiu Wang[1,2], Jingjing Jin[1], Bingcheng Si[1,2], Xiaojun Ma[3], Mingyi Wen[1]

[1]Key Laboratory of Agricultural Soil and Water Engineering in Arid and Semiarid Areas, Ministry of Education, Northwest A&F University, Yangling, Shaanxi Province 712100, China

[2]Department of Soil Science, University of Saskatchewan, Saskatoon SK S7N 5A8, Canada

[3]Gansu Provincial Department of Water Resources, Lanzhou, Gansu Province 730000, China

Correspondence to: Jingjing Jin (jin.jingjing1028@163.com)

Abstract. Soil evaporation is a key process in the water cycle and can be conveniently quantified with δ^2H and δ^{18}O in bulk surface soil water (BW). However, recent research shows that larger soil pore water evaporates first and differs from small pore water in δ^2H and δ^{18}O, which disqualifies quantification of evaporation from BW δ^2H and δ^{18}O. We hypothesize that BW has different isotopic compositions than evaporating water (EW). Therefore, our objectives are to test the hypothesis, and to evaluate if the difference alters the calculated evaporative water loss. We measured isotopic composition in soil water in two continuous evaporation periods in a summer maize field. Period I had a duration of 32 days following a precipitation event and Period II lasted 24 days following an irrigation event with a ^{2}H-enriched water. BW was obtained by cryogenically extracting water from samples of 0-5 cm soil taken every three days; EW was derived from condensation water collected every two days on plastic film placed on soil surface. Results showed that when newly added water was "heavier" than pre-event BW, δ^2H of BW in Period II decreased with the increase of evaporation time, indicating evaporation of heavy water; when newly added water was "lighter" than pre-event BW, δ^2H and δ^{18}O of BW in Period I and δ^{18}O of BW in Period II increased with increasing evaporation time, suggesting evaporation of light water. Moreover, relative to BW, EW had significantly smaller δ^2H and δ^{18}O in Period I and significantly smaller δ^{18}O in Period II (p<0.05). This suggests that evaporating water was newly added water, both of which were different from bulk soil water. Further, the newly added water may be in large pores, from which evaporation takes precedence. We also calculated soil evaporation losses from using water isotopes from EW and BW and they did not differ significantly (p>0.05). Our results have important implication for quantifying evaporation process with water stable isotopes.

1 Introduction

30 Terrestrial ecosystems receive water from precipitation and subsequently release all or part of the water to the atmosphere through transpiration from plant leaves and evaporation from soil surface. Evaporation from soils varies from 10 to 60 % of the total precipitation; and precisely estimating soil evaporative water loss relative to precipitation is critical to improve our knowledge of water budget, plant water use efficiency, global ecosystem productivity, the allocation of increasingly scarce water resources (Kool et

35 al., 2014; Oki and Kanae, 2006; Or et al., 2013; Wang et al., 2014) and calibrating hydrological and climate models (Or and Lehmann, 2019).

Water loss from soil progresses with air invasion into soil pores in an order from large to small (Aminzadeh and Or, 2014; Lehmann and Or, 2009; Or et al., 2013). Soil pores can be divided into large pores, medium pores, small pores, and film water space. The maximum film water amount is the residual

40 water content in soil characteristic curve (Van Genuchten, 1980; Zhang and Lockington, 2015). When larger soil pores are occupied by water, small pores water does not participate in evaporation (Or and Lehmann, 2019; Zhang and Lockington, 2015). Therefore, soil evaporation can be divided into three stages (Hillel, 1998; Or et al, 2013). Stage I: evaporation front is in the surface soil, large and medium pores water participate in evaporation, but larger pores are the primary contributor. With larger pores

45 water progressively depleted, the evaporation rate decreases gradually. Stage II: evaporation front is still in the surface soil, but larger pores are occupied by air, water residing in medium soil pores in the surface soil evaporates and deep larger soil pores recharge the surface medium pores by capillary pumping (Or and Lehmann, 2019); the evaporation rate remains constant. Stage III: the hydraulic connectivity between surface medium pores and deep large pores breaks, so evaporation front recedes into deep soil. Surface

50 small pore water and medium pore water on the evaporation front evaporate. The evaporation rate drops to a low value.

Furthermore, due to the low water potential, small soil pores in a dry soil are filled with infiltration water firstly (Beven and Germann, 1982; Brooks et al., 2010). But when small pores are filled with water, the infiltration water from precipitation or irrigation water goes into large pore preferentially and bypasses

55 the saturated smaller pores (Beven and Germann, 1982; Booltink and Bouma, 1991; Sprenger and Allen, 2020). As larger pores have larger hydraulic conductivity, water residing in larger pores drains firstly. Conversely, water residing in small pores drains lastly (Gerke and Van Genuchten, 1993; Phillips, 2010;

Van Genuchten, 1980). Therefore, small pore water has a longer residence time in the soil (Sprenger et al., 2019b).

60 The sequence of water invasion and depletion could introduce variability in isotopic composition between soil pore space. As is well-known, there are seasonal, temperature, and amount effects of local precipitation events, causing strong temporal variation in the isotopic composition of precipitation (Kendall and McDonnell, 2012). As a result, the different precipitation events having different isotopic compositions recharge different soil pores, which may yield differing isotopic compositions between

65 small pore water and large pore water (Brooks et al., 2010; Goldsmith et al., 2012; Good et al., 2015). And isotopically, small pore water may be similar to old precipitation and large pores water resembles new precipitation (Sprenger et al., 2019a; Sprenger et al., 2019b). In addition, mineral-water interaction, soil particle surface adsorption, and soil tension may also cause isotopic variation in soil pore space (Gaj et al., 2017a; Gaj and McDonnell, 2019; Oerter et al., 2014; Orlowski and Breuer, 2020; Thielemann et

70 al., 2019).

Despite of these recent progresses in understanding evaporation process and isotope partition in pore spaces, the latter, to our best knowledge, is not considered in soil evaporation calculation. The isotopic composition of bulk soil water - that is extracted by cryogenic vacuum distillation and containing both large and small pores water - is still routinely used in the evaporation calculation through Craig-Gordon

75 models (Allison and Barnes, 1983; Dubbert et al., 2013; Good et al., 2014; Robertson and Gazis, 2006; Sprenger et al., 2017). This may bias the evaporation estimates, because of isotopic variation in pore space and preference of larger pore water by evaporation.

Therefore, we hypothesize that the isotopic composition in evaporating water (EW) is similar with that of larger pores water but differs from that in BW; thus, evaporative water loss based on isotope value in

80 BW will be biased. The objectives of this study were to verify 1) if isotopic compositions differ between EW and BW; 2) if the isotopic composition difference substantially bias the calculated evaporative water loss. We obtained water isotopic compositions in BW by cryogenically extracting water from 0-5 cm soil samples and EW derived from condensation water on the plastic film in two continuous evaporation periods in a maize field using a randomized replication design. This study may better understand the

85 process of soil evaporation and the ecohydrological water cycle.

2 Material and methods

2.1 Experimental site

The field experiment was conducted from June to September of 2016 at Huangjiabao Village (34°17′ N, 108°05′ E, 534 m above sea level), located in the south Chinese Loess Plateau. The area experiences

90   temperate, semi-humid climate with a mean annual temperature of 13 ℃, precipitation of 620 mm and potential evaporation of 1,400 mm (Liang et al., 2012). Winter wheat followed by summer maize rotation is the routine practice in the region (Chen et al., 2015).

2.2 Experimental design

A summer maize field (35 m long and 21 m wide) was selected for this study. On 2016/6/18, maize seeds

95   were sown in alternating row spaces of 70 cm and 40 cm with 30 cm seed intervals in each row. Seeds were planted at the 5 cm depth beneath soil surface by a hole-sowing machine. The field was irrigated 30 mm of mixed tap water and deuterium enriched water (the ^{2}H concentration was 99.96 %, Cambridge Isotope Laboratories, Inc.) on 2016/8/26. The δ^2H and δ^{18}O in the irrigation water were 51.12±2.7 ‰ and -9.40±0.05 ‰ (Mean±SE, n=5), respectively.

100   ### 2.3 Samples collection and measurement

In order to determine the water isotopic composition in EW from condensation water of the evaporation vapor, we randomly selected three rectangular areas of 40 cm long and 30 cm wide. A channel of 3 cm deep was dug around the edge of the area (Fig. 1). Subsequently, a piece of plastic film without hole (about 0.2 m^2, 40 cm by 50 cm) was used to cover the soil surface, with an extra 5 cm at each side. Then

105   the channels were back filled with soil to keep the covered area free of the effect of wind. After equilibrium for two days, the condensation water adhered on the underside of the plastic film was collected using an injection syringe in the early morning at about 7 a.m. to eliminate the second-evaporation of the condensation water (Fig. 1), and transferred into a 1 mL glass vial. We assume that the condensation water is in constant equilibrium with evaporating water in soil and thus the water

110   isotopes of evaporating water in soil can be obtained from that of condensation water on the plastic film. After the collection, the plastic film was removed with little disturbance to the site. Subsequently, three new areas were selected randomly and covered in a similar manner with a new piece of plastic film for

the next water collection.
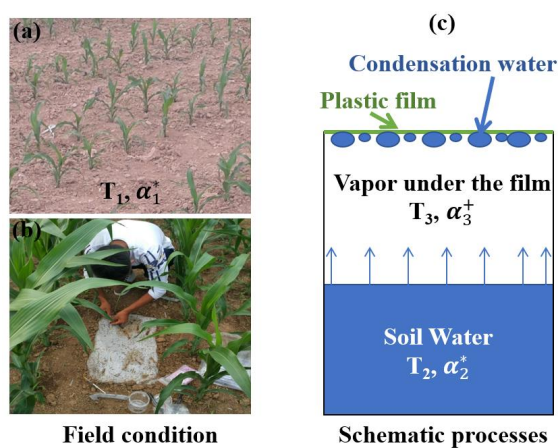
T_1: Soil temperature T_2: Soil temperature under film
T_3: Vapor temperature under film
α_1^*: Equilibrium fractionation factor in soil
α_2^*: Equilibrium fractionation factor in soil under film
α_3^+: Equilibrium fractionation factor in vapor under film

Figure 1: Photos of field condition (a), new plastic film cover and condensation water collection using a syringe (b), and schematic of condensation process (c).

In addition, BW was obtained from 0-5 cm surface soil water (Wen et al., 2016). The 0-5 cm soil samples were collected using a soil auger every three days with three replicates, and each was well mixed and separated into two subsamples: one for determining the soil gravimetric water content and the other for water stable isotope analysis. The subsample for soil gravimetric water content was stored in aluminum box and oven dried for 24 h at 105 °C. The other one was stored in 150 mL high density polyethylene bottles, sealed with parafilm®, transported to a freezer at -20 °C in the laboratory until cryogenic liquid water extraction took place. A cryogenic vacuum distillation system (LICA, Li-2000, China) with a pressure about 0.2 Pa and heating temperature at 95 °C was used to extract soil water (Wang et al., 2020). The extraction time was at least 2 h until all water evaporated from the soil and deposited to the cryogenic tube. In order to calculate the extraction efficiency, samples were weighed before and after extraction, and weighed again after oven-dried 24 h following extraction. Samples with an extraction efficiency less than 98 % were discarded. In terms of weight, the cryogenic vacuum distillation extracts all the water from soil. However, spiking experiments show that the extracted water is depleted in heavy isotope than the spiking water and the depletion is positive with increasing soil clay contents but negative with

increasing water contents. Moreover, higher temperature (>200 ºC) is suggested to be used for soil water extractions (Gaj et al., 2017a; Gaj et al., 2017b; Orlowski et al., 2018; Orlowski et al., 2016; Orlowski et al., 2013). Therefore, the water isotopic compositions obtained from our distillation system were subsequently corrected by a calibration equation. The equation contains clay and soil water content as

135 factors and was obtained through a spiking experiment with 205 ºC oven-dried soils (the related data was submitted to *Hydrological Processes*, under review).

Five deep soil profiles were collected on 2016/7/17, 2016/8/3, 2016/8/17, 2016/9/1, and 2016/9/16 with increments of 0-5, 5-10, 10-20, 20-30, 30-40, 40-60 cm. These soil samples were used to measure soil water contents and isotopic composition. Further, lc-excess of the soil before the enriched ^{2}H irrigation

140 was calculated to infer the evaporation enrichment to soil water. More negative lc-excess value indicates stronger evaporation effect (Landwehr and Coplen, 2006).

$$lc - excess = \ \delta^2 H - a\delta^{18}O - b \ , \hspace{3cm} (1)$$

where δ^2H and $\delta^{18}O$ are the soil water isotopic compositions; a and b are the slope and intercept of local meteoric water line, respectively.

145 Precipitation was collected during the whole growth season by three rainfall collectors (Wang et al., 2010) in the experimental field. The rainfall amount was obtained by weighing using an electrical balance. Subsequently, subsample of these rainfall samples were transferred to 15 mL glass vials and sealed immediately with parafilm® and placed in a refrigerator at 4 ºC.

The air and 0-5 cm soil temperature under the newly covered plastic film during 2016/9/10 to 2016/9/28

150 were measured by E-type thermocouple (OMEGA, USA) with a CR1000 datalogger and 0-5 cm soil temperature in field condition during the whole field season was measured by ibutton (Maxim Integrated, DS1921G, USA) with the frequency of one hour. We estimated 0-5 cm soil temperature under the newly covered plastic film before 2016/9/10 from the temperature of 0-5 cm soil without the plastic film covering through regression. The regression was established using 0-5 cm soil temperature under the

155 newly covered plastic film and soil temperature without plastic film covering between 2016/9/10 to 2016/9/28 using ibutton. Similarly, air temperature under the newly covered plastic film before 2016/9/10 was calculated from the temperature of 0-5 cm soil under the newly covered plastic film by regression between air temperature and 0-5 cm soil temperature under the newly covered plastic film. The regression equations were presented in the Supplement File. Moreover, the hourly ambient air relative humidity was

160   recorded by an automatic weather station (HOBO event logger, USA) located nearby at a distance of 3

km.

A micro-lysimeter (Ding et al., 2013; Kool et al., 2014) with three replicates, made of high-density

polyethylene with 10 cm in depth, 5.2 cm in inner radius, and 3 mm in thick, was used to obtain soil

evaporation amount. The micro-lysimeter was pushed into the soil surface between maize rows to retrieve

165   an undisturbed soil sample. Subsequently, we sealed the bottom, weighed the micro-lysimeter, placed it

back in the soil with the same level with soil surface, and no other sensor was installed. After two days'

evaporation, we weighed it again. The mass difference was the soil evaporation amount. Further, the soil

of the inside lysimeter was changed every four days. In addition, after every rainfall or irrigation, the soil

inside the micro-lysimeter was changed immediately.

170   At the end of growing season, stainless rings with the volume of 100 cm^3 were pushed into the soil to

obtain the soil samples. Subsequently, the soil samples were oven-dried and weighed. The bulk soil

density was obtained by dividing the dry soil mass by volume.

All the water samples were analyzed for δ^2H and δ^{18}O using isotopic ratio infrared spectroscopy (Los

Gatos Research, IWA (Model)-45EP, USA) at Northwest A&F University, China. The precision of this

175   machine is 1.0‰ and 0.2‰ for δ^2H and δ^{18}O, respectively.

The results are reported in δ-notation relative to V-SMOW as detailed in Equation (2).

$$\delta = \left(\frac{R_{sample}}{R_{standard}} - 1 \right) \times 1000 \text{ ‰} \ , \tag{2}$$

where R_{sample} denotes the ratio of the number of heavy isotopes to that of the light one in sample water;

$R_{standard}$ denotes the ratio in the Vienna Standard Mean Ocean Water (V-SMOW).

180   **2.4 Equilibrium fractionation processes**

Isotopic composition of EW was calculated from that of the condensation water that was adhered on the

underside of the newly covered plastic film. We assumed that the water vapor under newly covered plastic

film, and above the surface soil constitutes a closed system. Within the system, two equilibrium

fractionation processes are temperature-dependent and occur independently: Evaporation from surface

185   soil water to air under the plastic film occurs during the day time (8 a.m. to 8 p.m., Fig. 2), condensation

from the water vapor under the plastic film to liquid water ensued at night time (8 p.m. to 8 a.m.), and

the resulting dews (condensation water) were adhered on plastic film. The average temperatures for 8

a.m. to 8 p.m. and 8 p.m. to 8 a.m. of the day before water collection were used to calculate the

equilibrium fractionation factor (α) (Horita and Wesolowski, 1994) for evaporation and condensation

190 process, respectively.

$$1000 \times ln\alpha^+ (2H) = \frac{1158.8 \times T^3}{10^9} - \frac{1620.1 \times T^2}{10^6} + \frac{794.84 \times T}{10^3} - 161.04 + \frac{2.9992 \times 10^9}{T^3} \ , \tag{3}$$

$$1000 \times ln\alpha^+ (18O) = -7.685 + \frac{6.7123 \times 10^3}{T} - \frac{1.6664 \times 10^6}{T^2} + \frac{0.35041 \times 10^9}{T^3} \ , \tag{4}$$

$$\alpha^+ = \frac{\delta_{liquid} + 1000}{\delta_{vapor} + 1000} \ , \tag{5}$$

$$\alpha^* = 1/\alpha^+ \ , \tag{6}$$

195 where α^+ and α^* are the equilibrium fractionation factor during condensation and evaporation,

respectively; δ_{liquid} is the isotopic composition in the liquid water, δ_{vapor} is the isotopic composition in

the vapor, T is temperature presented in Kelvin.
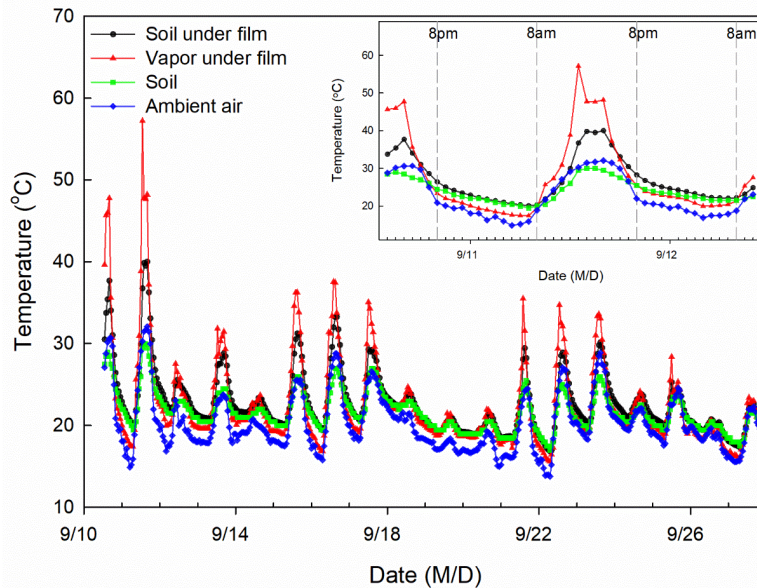
Figure 2: Temporal temperature variation of 0-5 cm soil in field condition (green), 0-5 cm soil under newly

200 **covered plastic film (black), vapor under newly covered plastic film (red), and ambient air (blue).**

Based on Eqs. (3-6) and Fig. 1c, the fractionation factors for two processes under the newly covered

plastic film are expressed using equations 7 and 8.

$$\alpha_2^* = \frac{\delta_{EW} + 1000}{\delta_{Vp} + 1000} \ , \tag{7}$$

$$\alpha_3^+ = \frac{\delta_{CW}+1000}{\delta_{Vp}+1000} \; , \tag{8}$$

205 where δ_{Vp} represents isotope values of vapor water under the newly covered plastic film, δ_{EW} represents

the isotope value in evaporating water, and δ_{CW} represents the isotope value in condensation water.

Combining equations (7) and (8), we obtained the isotopic composition in the EW:

$$\delta_{EW} = \frac{1}{\alpha_2^* \alpha_3^+}(\delta_{CW}+1000)\text{-}1000 \; , \tag{9}$$

2.5 Evaporative water losses

210 The evaporative water losses were estimated using Eqs. (10-18) (Hamilton et al., 2005; Skrzypek et al.,

2015; Sprenger et al., 2017), which is based on water balance and Craig-Gordon model.

$$f = 1 - \left[\frac{\delta_{BW}-\delta^*}{\delta_I-\delta^*}\right]^{\frac{1}{m}} \; , \tag{10}$$

where

$$m = \frac{h-\frac{\varepsilon}{1000}}{1-h+\frac{\varepsilon_k}{1000}} \; , \tag{11}$$

215 $$\delta^* = \frac{h*\delta_A+\varepsilon}{h-\frac{\varepsilon}{1000}} \; , \tag{12}$$

$$\varepsilon = \varepsilon^* + \varepsilon_k \; , \tag{13}$$

$$\varepsilon^* = (1-\alpha_1^*)*1000 \; , \tag{14}$$

$$\varepsilon^+ = (\alpha_A^+ - 1)*1000 \; , \tag{15}$$

$$\varepsilon_k(18O) = 28.5(1-h) \; , \tag{16}$$

220 $$\varepsilon_k(2H) = 25.115(1-h) \; , \tag{17}$$

$$\delta_A = (\delta_{rain} - \varepsilon^+)/\alpha_A^+ \; , \tag{18}$$

where f represents the ratio of evaporative water loss to the total water source; α_1^* is the equilibrium

fractionation factor in the soil; α_A^+ is the equilibrium fractionation factor in the ambient air; h is the

average ambient air relative humidity over 30 days prior to each soil water sampling (Sprenger et al.,

225 2017); δ_{rain} is the amount weighted isotopic composition in precipitation from 2016/7/11 to 2016/9/16;

δ_{BW} is the isotopic signal of 0-5 cm bulk soil water; δ_I is defined as the isotopic signal of the original

water source by calculating the intercept between the evaporation line of the 0-5 cm bulk soil water

isotope data in Period I in the dual-isotope plot and the LMWL (Fig. 3).
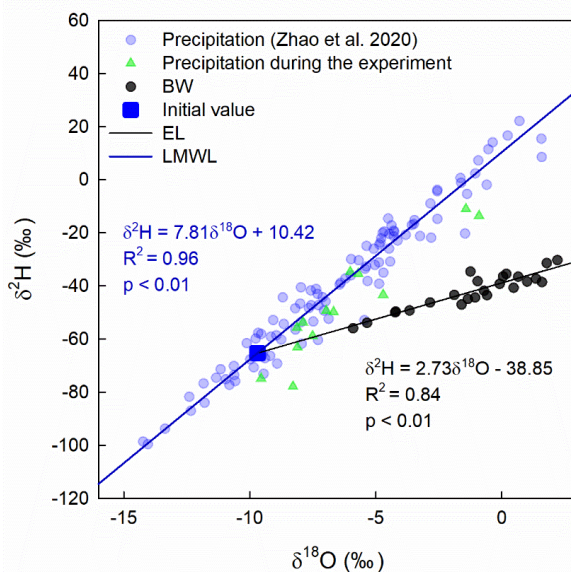
Figure 3: The dual-isotope plot of precipitation and 0-5 cm bulk soil water from 2016/7/25 to 2016/8/25. The regression for precipitation represents Local Meteoric Water Line (LMWL). The regression for bulk soil water (BW) represents Evaporation Line (EL).

To obtain the local meteoric water line (LMWL), we used three years of precipitation isotope data (Zhao et al., 2020) from 2015/4/1 to 2018/3/19. The equation of LMWL was $\delta^2H=7.81\ \delta^{18}O+10.42$.

In Period II, the initial value was calculated from the amount weighted average of the isotope values of irrigation water and Period I original water described above. In order to calculate evaporative water loss from EW $\delta^{18}O$, we used BW to express EW and obtained the following formulas (Eqs. 19-20) for evaporation fraction.

$$f = 1 - \left[\frac{\delta_{BW} - \delta^* + n}{\delta_I - \delta^* + n}\right]^{\frac{1}{m}}, \tag{19}$$

$$n = \frac{-2.13\alpha^*}{h - \frac{\varepsilon}{1000}}, \tag{20}$$

2.6 Statistical Analysis

General linear model (GLM) was used to test if the regression lines of isotopic composition/evaporative water loss of BW as a function of days after precipitation/irrigation (DAP/I) differs from that of EW. GLM was also used to compare Period I evaporative water loss derived from δ^2H and $\delta^{18}O$ of BW.

Shapiro-Wilk test was used to test the normality of the error structure of a model (p>0.05). Further,

Student's t test (Knezevic, 2008) was used to compare mean values.

3 Results

3.1 Variation of 0-5 cm soil water content

Between the two large precipitation events on 2016/7/24 and 2016/9/20, there was no effective

250   precipitation, except an irrigation event of 30 mm on 2016/8/26 (Fig. 4a). Thus, two continuous

evaporation periods can be identified: Period I was from 2016/7/25 to 2016/8/25, and Period II was from

2016/8/27 to 2016/9/19.
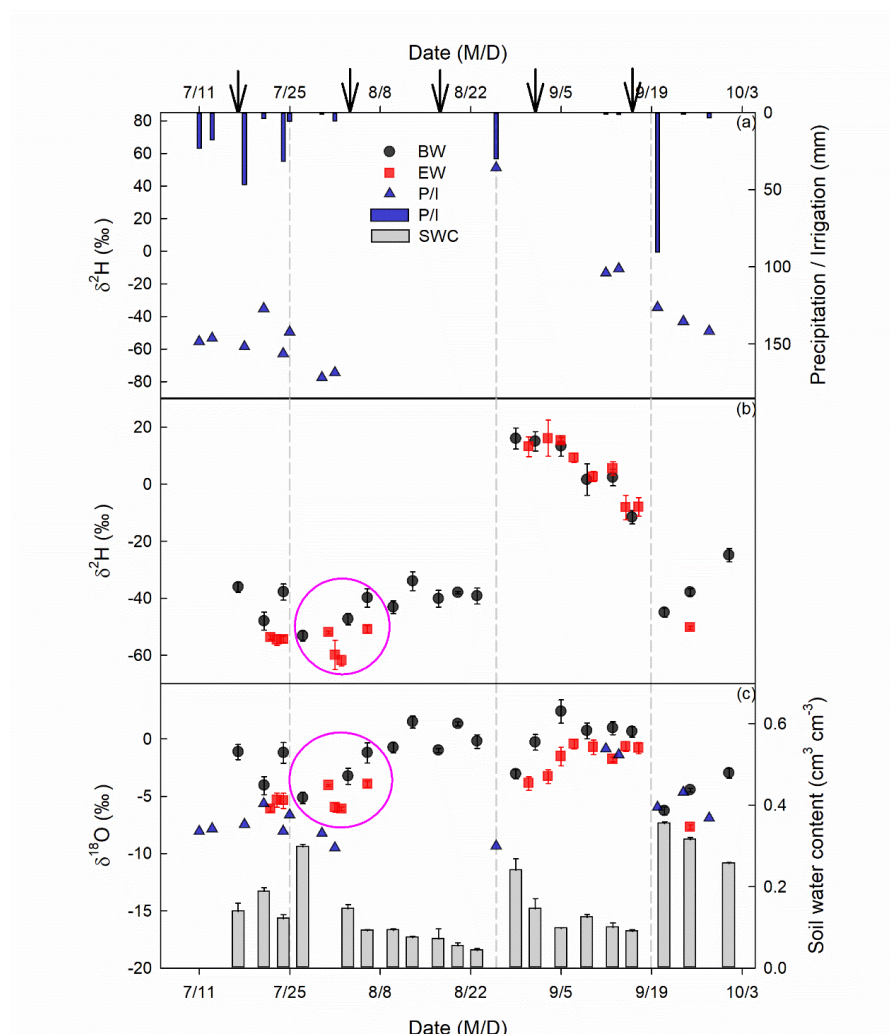
Figure 4: Temporal variation of water stable isotopic compositions (upper panel for δ^2H, lower panel for $\delta^{18}O$)

in different water bodies and the dynamics of precipitation/irrigation amount (P/I, blue bars) and 0-5 cm soil

water content (SWC, grey bars). 0-5 cm bulk soil water (BW, black dots), evaporating water (EW, red squares),

precipitation (P/I, blue upward-triangles). The precipitation on 2016/8/26 represents irrigation. The values

are expressed in Mean±SE. Moreover, two evaporation periods are indicated by three dashed grey lines.

Period I is from 2016/7/25 to 2016/8/25 and Period II is from 2016/8/27 to 2016/9/19. The isotopic composition

of BW and EW in Period I was compared by the mean value indicated by the pink circle with δ^2H -46.80±1.07,

-56.14±2.06 and $\delta^{18}O$ -3.21±0.32, -5.03±0.18 for BW and EW, respectively. The dates that deep soils were taken

are indicated by black arrows.

Figure 4 shows that the soil water content in 0-5 cm was close to saturation right after the first large

precipitation event (2016/7/24) and then decreased with evaporation time (grey bars in Fig. 4c). Similarly,

after the irrigation event (2016/8/26), 0-5 cm soil water content jumped to a high value and then decreased

with the increase of evaporation time (Fig. 4c). In total, there were 12.73±0.58 mm and 7.51±1.24 mm

reduction of soil water storage in 0-5 cm during Period I and Period II, respectively. However, from the

micro-lysimeters, we obtained the total evaporation amount of 20.45±0.95 mm in Period I, and 9.56±1.18

mm in Period II. Therefore, the evaporation amount in each of the two periods was larger than the soil

water storage reduction in 0-5 cm, suggesting soil water from below 5 cm moved up and was participated

in evaporation in each of the two periods, especially in Period I.

3.2 δ^2H and $\delta^{18}O$ in evaporating water and bulk soil water

The precipitation on 2016/7/24 had a $\delta^{18}O$ value of -8.11±0.05‰ and δ^2H value of -62.97±0.20‰, which

were smaller than the respective values of pre-event BW (-1.22±0.91‰ for $\delta^{18}O$ and -37.79±2.81‰ for

δ^2H) (Fig. 4). The irrigation water - with a $\delta^{18}O$ of -9.40±0.05‰ and δ^2H of 51.12±2.7‰ on 2016/8/26 -

had a lower $\delta^{18}O$, but a much higher δ^2H than the pre-irrigation BW (-0.22±0.59‰ for $\delta^{18}O$ and -

39.21±2.81‰ for δ^2H). Therefore, in Period I, the newly added water was more depleted in heavy

isotopes relatively to pre-event BW (p<0.05). In Period II, the newly added water had a lower $\delta^{18}O$, but

a higher δ^2H than pre-event BW (p<0.05).

As expected, the δ^2H and $\delta^{18}O$ in BW increased as evaporation occurred in Period I (p<0.05). The

increase of δ^2H and $\delta^{18}O$ in BW had a significant linear relationship with evaporation time (p<0.05; Fig.

5). This suggests that evaporation favored lighter water isotopes of both O and H from BW, resulting in

greater δ^2H and $\delta^{18}O$ in BW.
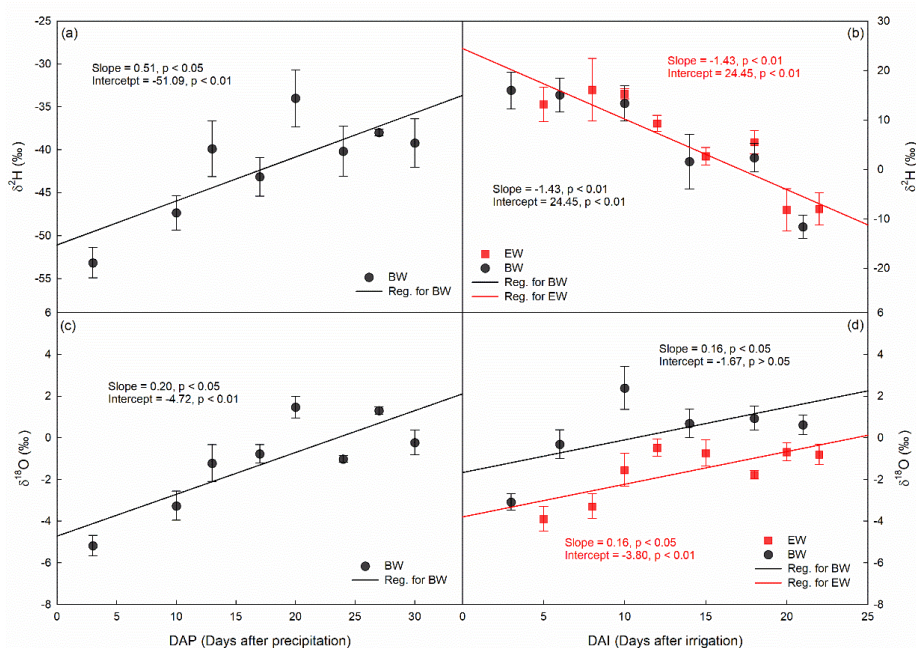
Figure 5: Temporal variation of δ^2H (upper panel) and $\delta^{18}O$ (lower panel) in 0-5 cm bulk soil water (black circles) and evaporating water (red squares) during Period I (left column) and Period II (right column). The precipitation happened on 2016/7/24, and the irrigation happened on 2016/8/26. All the regressions were produced by the function of glm() in R and the slopes and intercepts and their significances are indicated in the figure. The values are expressed in Mean±SE.

In Period II, BW $\delta^{18}O$ also increased as evaporation occurred ($p<0.05$). The increase of BW $\delta^{18}O$ also had a significant linear relationship with evaporation time ($p<0.05$; Fig. 5). On the contrary, δ^2H of BW, surprisingly decreased linearly with evaporation ($p<0.01$). The slope and intercept were both significantly different from zero ($p<0.01$). This suggests that in Period II evaporation favors the lighter isotope for O, but heavier isotope for H.

The change of water isotopes in EW is very similar to that in BW. For example, in Period II, water isotopes in EW showed a similar trend as in BW: $\delta^{18}O$ increased with evaporation time (Fig. 5d) and the slope and intercept were significantly different from zero ($p<0.05$). And $\delta^{18}O$ was consistently more depleted in EW than in BW in the period with same slope but significantly smaller intercept ($p<0.01$). Also similar to that in BW, δ^2H in EW decreased with evaporation time but did not differ from that in

BW (p>0.05, Figs. 4, 5), therefore the two lines had the similar slope and intercept (Fig. 5b). Therefore, the linear relationship in δ^{18}O between EW and BW was given as:

δ^{18}O(EW) = δ^{18}O(BW)-2.13 (Fig. 5)

While the slopes represent the evaporative demand of the atmosphere, regardless of the source of water, the intercept represents the initial condition of the source of water for evaporation. Therefore, the initial water source in Period II had a δ^{18}O value of -1.67‰ for BW, but of -3.80‰ for EW. Therefore, the sources of water for BW and EW had different isotopic compositions in Period II.

3.3 Variation of deep soil water content, δ^2H, δ^{18}O, and lc-excess

The precipitation on 2016/7/24 increased the soil water content in the top 60 cm, but decreased soil water δ^2H and δ^{18}O in the top 20 cm (Fig. 6, upper panel). Therefore, the top 20 cm lc-excess on 2016/8/3 increased. However, the precipitation had no influence on deeper soil δ^2H, δ^{18}O, and lc-excess. At the end of evaporation Period I, soil water content decreased in the top 60 cm. And in the top 10 cm, soil water δ^2H and δ^{18}O increased and lc-excess decreased.
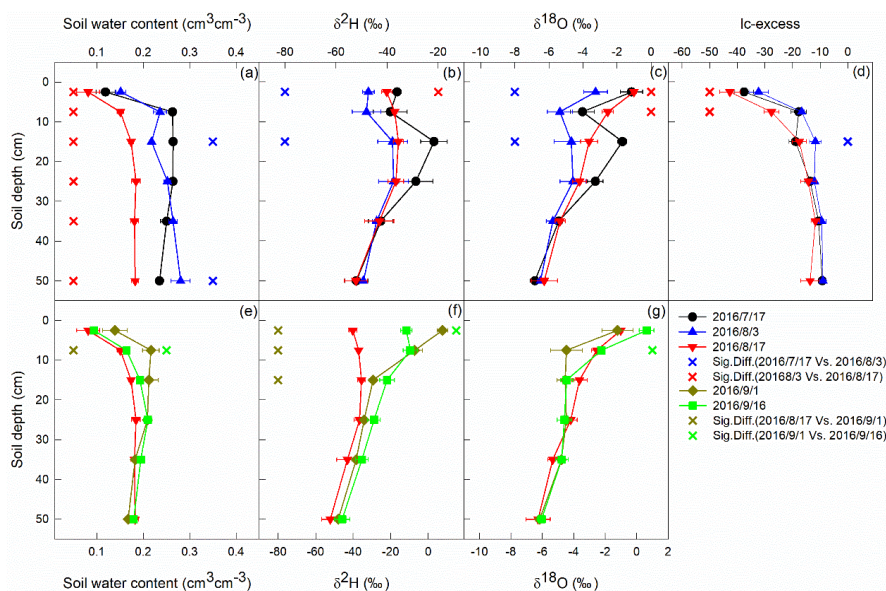
Figure 6: Temporal variation of deep soil water content, δ^2H, δ^{18}O, and lc-excess. Upper panel represents before (2016/7/17, black circles) and during Period I (2016/8/3, blue upward-triangles; 2016/8/17, red downward-triangles). Lower panel represents before (2016/8/17, red downward-triangles) and during Period II (2016/9/1, yellow diamonds; 2016/9/16, green squares). The significant difference (p<0.05) between

2016/7/17 and 2016/8/3, 2016/8/3 and 2016/8/17, 2016/8/17 and 2016/9/1, and 2016/9/1 and 2016/9/16 are represented by blue, red, yellow, and green crosses, respectively.

320   Similar with precipitation on 2016/7/24, the irrigation on 2016/8/26 increased soil water content and decreased $\delta^{18}O$ of top 10 cm soil (Fig. 6, lower panel). However, the irrigation event increased the δ^2H in the top 20 cm. At the end of evaporation Period II, the top 10 cm soil water $\delta^{18}O$ became more enriched, but δ^2H became more depleted. Note that δ^2H of 5-10 cm was similar to that of 0-5 cm (Fig. 6f).

3.4 Evaporative water loss derived from bulk soil water and evaporating water

325   In Period I, evaporative water loss (f) derived from either δ^2H or $\delta^{18}O$ in BW increased with increasing evaporation time (p<0.01), and there was no significant difference between them with the same slope and similar intercepts (p>0.05, Fig. 7). The average f values during the period were 0.27±0.004 and 0.23±0.002 for δ^2H and $\delta^{18}O$, respectively. In Period II, f derived from $\delta^{18}O$ in BW and EW increased with evaporation time (p<0.05), and there was no significant difference between them with the same

330   slope and similar intercepts (p>0.05). The average f was 0.27±0.01 and 0.24±0.01 for BW and EW, respectively. However, the evaporative water loss could not be calculated from δ^2H in BW or EW, as δ^2H decreased with on-going evaporation (Fig. 5), which were inconsistent with the evaporation theory that soil evaporation enriches heavier water isotopes in the residual soil water.
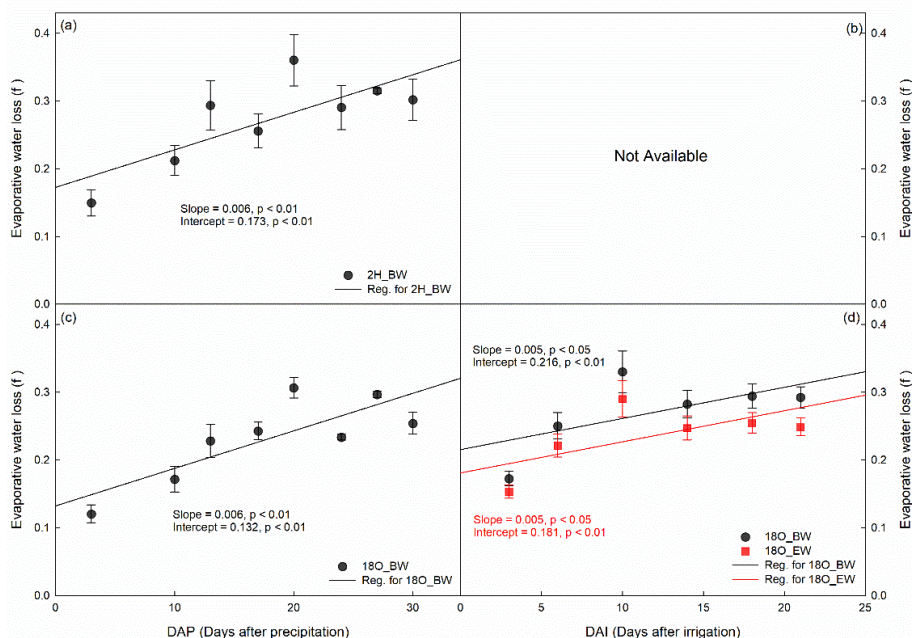
Figure 7: Temporal variation of evaporative water loss (*f*) derived from isotope value (δ^2H for upper panel and δ^{18}O for lower panel) in bulk soil water (BW, black circles) and evaporating water (EW, red squares) during Period I (left column) and Period II (right column). The precipitation happened on 2016/7/24, and the irrigation happened on 2016/8/26. The values are expressed in Mean±SE.

4 Discussion

4.1 Why evaporating and bulk soil water isotopic compositions differ

During evaporation, light isotopes are favored to the vapor making the residual liquid water enriched in heavy isotopes (Mook and De Vries, 2000). This can explain why, with increasing evaporation time, both δ^2H and δ^{18}O in BW experienced increasing trend in Period I. In Period II, δ^{18}O (Fig. 5) displayed a similar, increasing trend, but δ^2H had an opposite, decreasing trend. This is inconsistent with the trend, of δ^{18}O in the same period and, of both δ^2H and δ^{18}O in Period I (Fig. 5). The progressive decrease in δ^2H with increasing evaporation time cannot be explained by the general notion that with evaporation, residual soil water becomes more enriched with heavy water isotopes. Therefore, there must be a mechanism that either preferentially removes ^{2}H or dilutes ^{2}H by ^{2}H-depleted water.

For the latter, because there is negligible input of water from the atmosphere (both in vapor and liquid

350   form), the only input of water could be from the soil below 5 cm. Indeed, because the evaporation amount,

derived by lysimeters, was larger than 0-5 cm soil water storage reduction (Sect. 3.1), the water below 5

cm must have moved upward as evaporation occurred. Consequently, due to evaporation, the order of

δ^2H value should be 0-5 cm > the mixture of pre-evaporation 0-5 cm and 5-10 cm soil water > 5-10 cm.

However, 0-5 cm δ^2H at the end of evaporation period, i.e. on 2016/9/16, is similar to 5-10 cm δ^2H (Fig.

355   6f). Moreover, if dilution occurred, the δ^{18}O would also be diluted, which is not supported by the

progressive increase of BW δ^{18}O during evaporation in the same period and of both δ^2H and δ^{18}O in BW

of Period I, which should have more deep soil water contribution (Sect. 3.1). Therefore, dilution should

not have substantially affected the isotopic signature of BW. This is further supported by the larger δ^{18}O

in BW in Period II than that in EW (Figs. 4, 5). By deduction, the possible cause of the depletion in ^{2}H

360   would be a preferential removal of ^{2}H from the top 5 cm of soil.

We did not detect significant δ^2H differences in EW from that in BW in Period II (Fig. 5). However, there

was a significant δ^{18}O difference in Period II and both δ^2H and δ^{18}O difference in Period I (Figs. 4, 5).

Different isotopic signatures of BW and EW indicates that the sources of water for BW and EW were

different. The source of EW is closer to new water than that of BW. This could be explained by a

365   conceptual model of new water and old water partition in soil (Fig. 8).
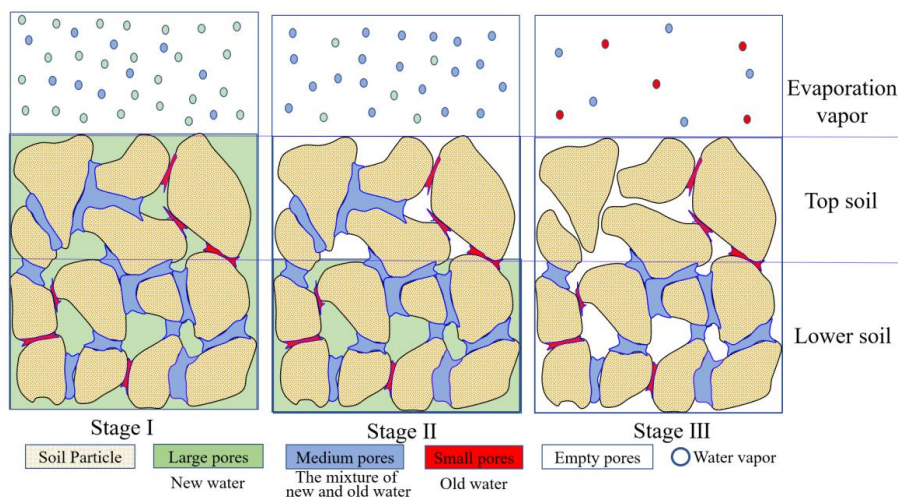
Figure 8: Schematic of soil pores water partition during evaporation.

As pointed out abundantly in the recent literature, there could be isotopic separation in water isotopes

between large pores and small pores (Brooks et al., 2010; Goldsmith et al., 2012; Good et al., 2015;
370   Sprenger et al., 2019a). The irrigation water would first enter large pores, because small pores are
occupied by bound water and large pores are empty (Beven and Germann, 1982; Gerke and Van
Genuchten, 1993; Sprenger et al., 2019a). Water flow is much faster in large pore than in small pores
(Van Genuchten, 1980). As a result, irrigation water first enters large pores, bypassing small pores. This
creates separation between small pores and large pores, with new water in large pores and pre-event water
375   in small pore. Based on this assumption, we establish a conceptual model for water in soil pores (Fig. 8).

4.2 Conceptual model for water partition in large pores and small pores during evaporation

For large precipitation events, new event water will infiltrate into the empty large pore preferentially due
to the large hydraulic conductivity associated with large pores, and then transfer some of the water to the
surrounding empty small pores, bypassing water-occupied small soil pores in soil matrix (Beven and
380   Germann, 1982; Booltink and Bouma, 1991; Weiler and Naef, 2003). In our experiment, the precipitation
event on 2016/7/24 was 31 mm, and the irrigation event on 2016/8/26 was 30 mm, and both are large
events. Because small pores are prefilled by pre-event water, we assume that large pores will be filled by
the new water; and medium pores are likely filled by the mixture of pre-event water and new water.
Therefore, water in large pores water is similar to the new precipitation and smaller pores water is close
385   to the older precipitation (Brooks et al., 2010; Sprenger et al., 2019a).

On the other hand, at the end of evaporation period, lc-excess of 0-5 cm soil on 2016/8/17, which had
the lower soil water content than that in Period II, was still the smallest comparing with deeper soil (Fig.
6d). Therefore, the evaporation front was in the surface soil for both Periods. Thus, the evaporation in
our experiment was in evaporation stage I or II as indicated in the introduction. During evaporation stage
390   I and II, small pores water does not evaporate (Or and Lehmann, 2019; Zhang and Lockington, 2015),
and larger pores water is the primary source of water for evaporation. As smaller pores can extract water
from larger pores via capillary pumping to recharge the evaporation depletion, the evaporation empties
the soil pores in the order from large to small pores (Lehmann and Or, 2009; Or et al., 2013).

Therefore, EW is large pore water, which is similar to the new water in isotopic composition; BW
395   contains the EW and evaporation-insulated small pores water, which is close to the old, pre-event water.
Compared with old water, new water takes precedence to be evaporated. Therefore, the sequence of water
in the evaporation layer can be analogically summarized as a "last-in-first-out" rule. Thus, when isotopic

composition in the newly added water was smaller than that in pre-event BW, such as δ^2H and $\delta^{18}O$ in

400   Period I and $\delta^{18}O$ in Period II, isotopic composition in EW was smaller than that in BW (Fig. 4). When

the newly added water was enriched in heavy isotope relatively to pre-event BW, such as δ^2H in Period

II, EW should be enriched in ^2H compared to BW; however, more precise analysis is needed.

Furthermore, evaporative enrichment and loss of large pore water both affect the temporal variation of

δ^2H and $\delta^{18}O$ in EW and BW. When large pore water is depleted in heavy isotope relatively to pre-event

water, isotopic composition in EW and BW increases with time; when large pore water is enriched in

405   heavy isotope relatively to pre-event water, the enriched water in larges pores empty first, leaving lighter

water molecules in BW, which will decrease the isotopic composition in EW and BW with evaporation

time.

4.3 Why the isotopic difference did not make a difference in estimated evaporative water loss?

There was a significant difference in isotopic composition of EW from BW; however, the evaporative

410   water loss derived from EW and BW did not differ ($p > 0.05$). As discussed above, the difference between

EW and BW is caused by the small pores water, which does not experience evaporation. The differences,

in Period II, was 2.13‰ for $\delta^{18}O$. Nevertheless, the difference in $\delta^{18}O$ of EW and BW is too small to

make a difference on the calculated evaporative water loss. However, by increasing the difference value

from 2.13 ‰ to 3.52 ‰, there will be a significant difference in the calculated evaporative water loss.

415   Therefore, more attention is needed when there is a large difference in isotopic composition between

newly added water and pre-event water. However, more precise analysis is needed when the difference

is too large to detect the difference in EW and BW as showed by our δ^2H result in Period II.

While evaporation prefers larger pore water, large pore water also has relatively high-water potential and

therefore, may also be preferred by roots and dominate groundwater recharge (Sprenger et al., 2018). In

420   other words, evaporation, transpiration, and groundwater preferentially tap the same pool of water - the

water that resides in large soil pores. This is consistent with the finding of Brooks et al. (2010) and can

have broad ecohydrological implications.

5 Conclusion

We did the experiment in two continuous evaporation periods: a relatively depleted water input in Period

425   I and more enriched ^{2}H and depleted ^{18}O water input in Period II. Using newly covered plastic film, we

collected the condensation water and calculated the evaporating water isotopic composition.

Results showed that δ^2H and δ^{18}O in EW had similar trend with that in BW. When new water was depleted

in heavy isotopes relatively to old pre-event water, isotopic composition in EW and BW increased with

increasing evaporation time ($p<0.05$), and EW was depleted in heavy isotopes relatively to BW ($p<0.05$).

430   When new water was enriched in heavy isotopes relatively to old water, isotopic composition in EW and

BW decreased with evaporation time increasing ($p<0.01$). Moreover, the average evaporative water loss

derived from δ^{18}O was 0.27 ± 0.01 and 0.24 ± 0.01 for BW and EW, respectively. The difference between

evaporative water loss was negligible due to the small difference in δ^{18}O of EW and BW. As the δ^2H in

BW and EW decreased with evaporation, we could not obtain the evaporative water loss using δ^2H. Our

435   results indicate that even isotopic composition in BW is significantly different from that in EW, the

difference does not affect evaporative water loss calculation. However, more attention is needed when

there is a large isotopic difference between new water and pre-event water. Our research is important for

better understanding soil evaporation process and using isotopes to study evaporation fluxes.

Data availability

440   The data that support the findings of this study are provided as Supplement.

Author contribution

H. Wang and J. Jin designed the research, prepared and interpreted the data, and wrote the manuscript.

B. Si and M. Wen offered constructive suggestions for the manuscript. H. Wang and X. Ma conducted

the fieldwork.

445   **Competing interests**

The authors declare that they have no conflict of interest.

Acknowledgement

This work was partially funded by the National Natural Science Foundation of China (41630860;

41371233) and Natural Science and Engineering Research Council of Canada (NSERC). We thank the

450 China Scholarship Council (CSC) for providing funds (201806300115) to Hongxiu Wang to pursue her

studies at the University of Saskatchewan, Canada. We thank Han Li for the fruitful discussion.

References

Allison, G. B. and Barnes, C. J.: Estimation of evaporation from non-vegetated surfaces using natural

455 deuterium, Nature, 301, 143-145, doi:10.1038/301143a0, 1983.

Aminzadeh, M. and Or, D.: Energy partitioning dynamics of drying terrestrial surfaces, J. Hydrol., 519, 1257-1270, doi:10.1016/j.jhydrol.2014.08.037, 2014.

Beven, K. and Germann, P.: Macropores and water flow in soils, Water Resour. Res., 18, 1311-1325, doi:10.1029/WR018i005p01311, 1982.

460 Booltink, H. W. G. and Bouma, J.: Physical and morphological characterization of bypass flow in a well-structured clay soil, Soil Sci Soc Am J, 55, 1249-1254, doi:10.2136/sssaj1991.03615995005500050009x, 1991.

Brooks, J. R., Barnard, H. R., Coulombe, R., and McDonnell, J. J.: Ecohydrologic separation of water between trees and streams in a Mediterranean climate, Nat. Geosci., 3, 100-104, doi:10.1038/NGEO722,

465 2010.

Chen, H., Zhao, Y., Feng, H., Li, H., and Sun, B.: Assessment of climate change impacts on soil organic carbon and crop yield based on long-term fertilization applications in Loess Plateau, China, Plant Soil, 390, 401-417, doi:10.1007/s11104-014-2332-1, 2015.

Ding, R., Kang, S., Li, F., Zhang, Y., and Tong, L.: Evapotranspiration measurement and estimation using

470 modified Priestley–Taylor model in an irrigated maize field with mulching, Agric For Meteorol, 168, 140-148, doi:10.1016/j.agrformet.2012.08.003, 2013.

Dubbert, M., Cuntz, M., Piayda, A., Maguás, C., and Werner, C.: Partitioning evapotranspiration–Testing the Craig and Gordon model with field measurements of oxygen isotope ratios of evaporative fluxes, J. Hydrol., 496, 142-153, doi:10.1016/j.jhydrol.2013.05.033, 2013.

475 Gaj, M., Kaufhold, S., Koeniger, P., Beyer, M., Weiler, M., and Himmelsbach, T.: Mineral mediated isotope fractionation of soil water, Rapid Commun. Mass Spectrom., 31, 269-280, doi:10.1002/rcm.7787,

2017a.

Gaj, M., Kaufhold, S., and McDonnell, J. J.: Potential limitation of cryogenic vacuum extractions and spiked experiments, Rapid Commun. Mass Spectrom., 31, 821-823, doi: 10.1002/rcm.7850, 2017b.

480   Gaj, M. and McDonnell, J. J.: Possible soil tension controls on the isotopic equilibrium fractionation factor for evaporation from soil, Hydrol Process, 33, 1629-1634, doi:10.1002/hyp.13418, 2019.

Gerke, H. H. and Van Genuchten, M. T.: A dual-porosity model for simulating the preferential movement of water and solutes in structured porous media, Water Resour. Res., 29, 305-319, doi:10.1029/92WR02339, 1993.

485   Goldsmith, G. R., Muñoz-Villers, L. E., Holwerda, F., McDonnell, J. J., Asbjornsen, H., and Dawson, T. E.: Stable isotopes reveal linkages among ecohydrological processes in a seasonally dry tropical montane cloud forest, Ecohydrology, 5, 779-790, doi:10.1002/eco.268, 2012.

Good, S. P., Noone, D., and Bowen, G.: Hydrologic connectivity constrains partitioning of global terrestrial water fluxes, Science, 349, 175-177, doi:10.1126/science.aaa5931, 2015.

490   Good, S. P., Soderberg, K., Guan, K., King, E. G., Scanlon, T. M., and Caylor, K. K.: $\delta 2H$ isotopic flux partitioning of evapotranspiration over a grass field following a water pulse and subsequent dry down, Water Resour. Res., 50, 1410-1432, doi:10.1002/2013WR014333, 2014.

Hamilton, S. K., Bunn, S. E., Thoms, M. C., and Marshall, J. C.: Persistence of aquatic refugia between flow pulses in a dryland river system (Cooper Creek, Australia), Limnol. Oceanogr., 50, 743-754,
495   doi:10.4319/lo.2005.50.3.0743, 2005.

Hillel, D.: Environmental soil physics: Fundamentals, applications, and environmental considerations, Elsevier, 1998.

Horita, J. and Wesolowski, D. J.: Liquid-vapor fractionation of oxygen and hydrogen isotopes of water from the freezing to the critical temperature, Geochim. Cosmochim. Acta, 58, 3425-3437,
500   doi:10.1016/0016-7037(94)90096-5, 1994.

Kendall, C. and McDonnell, J. J. (Eds.): Isotope tracers in catchment hydrology, Elsevier, 2012.

Knezevic, A.: Overlapping confidence intervals and statistical significance, StatNews: Cornell University Statistical Consulting Unit, 73, 2008.

Kool, D., Agam, N., Lazarovitch, N., Heitman, J. L., Sauer, T. J., and Ben-Gal, A.: A review of approaches
505   for   evapotranspiration   partitioning,   Agric   For   Meteorol,   184,   56-70,

doi:10.1016/j.agrformet.2013.09.003, 2014.

Landwehr, J. M. and Coplen, T. B.: Line-conditioned excess: a new method for characterizing stable hydrogen and oxygen isotope ratios in hydrologic systems, In International conference on isotopes in environmental studies, Vienna: IAEA, 132-135, 2006.

510 Lehmann, P. and Or, D.: Evaporation and capillary coupling across vertical textural contrasts in porous media, Phys. Rev. E, 80, 046318, doi:10.1103/PhysRevE.80.046318, 2009.

Liang, B., Yang, X., He, X., Murphy, D. V. and Zhou, J.: Long-term combined application of manure and NPK fertilizers influenced nitrogen retention and stabilization of organic C in Loess soil, Plant Soil, 353, 249-260, doi:10.1007/s11104-011-1028-z, 2012.

515 Mook, W. G. and De Vries, J. J.: Volume I, Introduction: theory methods review, Environmental Isotopes in the Hydrological Cycle—Principles and Applications, International Hydrological Programme (IHP-V), Technical Documents in Hydrology (IAEA/UNESCO) No, 39, 75-76, 2000.

Oerter, E., Finstad, K., Schaefer, J., Goldsmith, G. R., Dawson, T., and Amundson, R.: Oxygen isotope fractionation effects in soil water via interaction with cations (Mg, Ca, K, Na) adsorbed to phyllosilicate

520 clay minerals, J. Hydrol., 515, 1-9, doi:10.1016/j.jhydrol.2014.04.029, 2014.

Oki, T. and Kanae, S.: Global hydrological cycles and world water resources. Science, 313, 1068-107, doi:10.1126/science.1128845, 2006.

Or, D. and Lehmann, P.: Surface evaporative capacitance: How soil type and rainfall characteristics affect global-scale surface evaporation, Water Resour. Res., 55, 519-539, doi:10.1029/2018WR024050, 2019.

525 Or, D., Lehmann, P., Shahraeeni, E., and Shokri, N.: Advances in soil evaporation physics—A review, Vadose Zone J, 12, 1-16, doi:10.2136/vzj2012.0163, 2013.

Orlowski, N. and Breuer, L.: Sampling soil water along the pF curve for δ2H and δ18O analysis, Hydrol Process, 34, 4959-4972, doi:10.1002/hyp.13916, 2020.

Orlowski, N., Breuer, L., Angeli, N., Boeckx, P., Brumbt, C., Cook, C. S., ... and McDonnell, J. J.:

530 Interlaboratory comparison of cryogenic water extraction systems for stable isotope analysis of soil water, Hydrol Earth Syst Sci, 22, 3619-3637, doi:10.5194/hess-22-3619-2018, 2018.

Orlowski, N., Breuer, L., and McDonnell, J. J.: Critical issues with cryogenic extraction of soil water for stable isotope analysis, Ecohydrology, 9, 1-5, doi:10.1002/eco.1722, 2016.

Orlowski, N., Frede, H. G., Brüggemann, N., and Breuer, L.: Validation and application of a cryogenic

535   vacuum extraction system for soil and plant water extraction for isotope analysis, J. Sens. Sens. Syst., 2, 179-193, doi:10.5194/jsss-2-179-2013, 2013.

Phillips, F. M.: Soil-water bypass, Nat. Geosci., 3, 77-78, doi:10.1038/ngeo762, 2010.

Robertson, J. A. and Gazis, C. A.: An oxygen isotope study of seasonal trends in soil water fluxes at two sites along a climate gradient in Washington state (USA), J. Hydrol., 328, 375-387,
540   doi:10.1016/j.jhydrol.2005.12.031, 2006.

Skrzypek, G., Mydłowski, A., Dogramaci, S., Hedley, P., Gibson, J. J., and Grierson, P. F.: Estimation of evaporative loss based on the stable isotope composition of water using Hydrocalculator, J. Hydrol., 523, 781-789, doi:10.1016/j.jhydrol.2015.02.010, 2015.

Sprenger, M. and Allen, S. T.: What ecohydrologic separation is and where we can go with it, Water
545   Resour. Res., 56, e2020WR027238, doi:10.1029/2020wr027238, 2020.

Sprenger, M., Tetzlaff, D., and Soulsby, C.: Soil water stable isotopes reveal evaporation dynamics at the soil–plant–atmosphere interface of the critical zone, Hydrol Earth Syst Sci, doi:10.5194/hess-21-3839-2017, 2017.

Sprenger, M., Tetzlaff, D., Buttle, J., Laudon, H., and Soulsby, C.: Water ages in the critical zone of long-
550   term experimental sites in northern latitudes, Hydrol Earth Syst Sci, doi:10.5194/hess-22-3965-2018, 2018.

Sprenger, M., Llorens, P., Cayuela, C., Gallart, F., and Latron, J.: Mechanisms of consistently disconnected soil water pools over (pore) space and time, Hydrol Earth Syst Sci, 23, 1-18, doi:10.5194/hess-2019-143, 2019a.

555   Sprenger, M., Stumpp, C., Weiler, M., Aeschbach, W., Allen, S. T., Benettin, P., ... and McDonnell, J. J.: The demographics of water: A review of water ages in the critical zone, Rev. Geophys., 57, 800-834, doi:10.1029/2018rg000633, 2019b.

Thielemann, L., Gerjets, R., and Dyckmans, J.: Effects of soil-bound water exchange on the recovery of spike water by cryogenic water extraction, Rapid Commun. Mass Spectrom., 33, 405-410,
560   doi:10.1002/rcm.8348, 2019.

Van Genuchten, M. T.: A closed-form equation for predicting the hydraulic conductivity of unsaturated soils, Soil Sci Soc Am J, 44, 892-898, doi:10.2136/sssaj1980.03615995004400050002x, 1980.

Wang, H., Si, B., Pratt, D., Li, H., and Ma, X.: Calibration method affects the measured δ^2H and $\delta^{18}O$

in soil water by direct H2Oliquid–H2Ovapour equilibration with laser spectroscopy, Hydrol Process, 34,

565   506-516, doi:10.1002/hyp.13606, 2020.

Wang, L., Good, S. P., and Caylor, K. K.: Global synthesis of vegetation control on evapotranspiration

partitioning, Geophys. Res. Lett., 41, 6753-6757, doi:10.1002/2014gl061439, 2014.

Wang, P., Song, X., Han, D., Zhang, Y., and Liu, X.: A study of root water uptake of crops indicated by

hydrogen and oxygen stable isotopes: A case in Shanxi Province, China, Agric Water Manag, 97, 475-

570   482, doi:10.1016/j.agwat.2009.11.008, 2010.

Weiler, M. and Naef, F.: An experimental tracer study of the role of macropores in infiltration in grassland

soils, Hydrol Process, 17, 477-493, doi:10.1002/hyp.1136, 2003.

Wen, X., Yang, B., Sun, X., and Lee, X.: Evapotranspiration partitioning through in-situ oxygen isotope

measurements   in   an   oasis   cropland,   Agric   For   Meteorol,   230,   89-96,

575   doi:10.1016/j.agrformet.2015.12.003, 2016.

Zhang, C., Li, L., and Lockington, D.: A physically based surface resistance model for evaporation from

bare soils, Water Resour. Res., 51, 1084-1111, doi:10.1002/2014wr015490, 2015.

Zhao, M. H., Lu, Y. W., Rachana, H., and Si, B. C.: Analysis of Hydrogen and Oxygen Stable Isotope

Characteristics and Vapor Sources of Precipitation in the Guanzhong Plain, Chinese Journal of Huan Jing

580   Ke Xue, 41, 3148-3156, doi:10.13227/j.hjkx.201911063, 2020.